J. Plasma Fusion Res. SERIES, Vol. 9 (2010)

Pellet ablation in helical plasmas

Ryuichi ISHIZAKI and Noriyoshi NAKAJIMA
National Institute for Fusion Science, Toki 509-5292, Japan

(Received: 20 November 2009 / Accepted: 22 March 2010)

In order not only to clarify the difference on the motion of a plasmoid created by a pellet injection between tokamak and helical plasmas but also to obtain the universal understanding on the motion in torus plasmas, MHD simulations have been carried out in tokamak, vacuum toroidal field, RFP-like and LHD configurations. It is found that the plasmoids drift in the opposite direction of the curvature vector in tokamak, vacuum toroidal field and RFP-like configurations, but the plasmoid motions depend on the initial locations of plasmoids in LHD. It is also clarified that there are two main forces acting on the plasmoid, and the connection length determines which force is dominant on the plasmoid motion.

Keywords: pellet, ablation, MHD, LHD

1. Introduction

Injecting small pellets of frozen hydrogen into torus plasmas is a proven method of fueling [1]. The physical processes are divided into the following micro and macro stages. The micro stage is the ablation of mass at the pellet surface due to the high temperature bulk plasma which the pellet encounters. The neutral gas produced by the ablation is rapidly heated by electrons and ionized to form a high density and low temperature plasma, namely a plasmoid. The macro stage is the redistribution of the plasmoid by free streaming along the magnetic field lines and by MHD processes which cause mass flow across flux surfaces. The micro stage is well-understood by an analytic method [2] and numerical simulation [3]. The drift motion of the plasmoid is investigated in the macro stage [4]. Since the plasmoid drifts to the lower field side, the pellet fueling to make the plasmoid approach the core plasma has succeeded by injecting the pellet from the high field side in tokamak. On the other hand, such a good performance has not been obtained yet in the planar axis heliotron; Large Helical Device (LHD) experiments, even if a pellet has been injected from the high field side [5]. The purpose of the study is to clarify the difference on the motion of the plasmoid between tokamak and helical plasmas.

In order to investigate the motions of the plasmoids in tokamak and LHD, the three dimensional MHD code has been developed by extending the pellet ablation code (CAP) [3, 6]. Especially, since LHD has complicated magnetic field, the simulations have been carried out in three cases in which initial plasmoids are located inside and outside the torus on the horizontal elongated poloidal cross sections and inside the torus on the vertical elongated poloidal cross section. In addition, in order to obtain the universal understanding in torus plasmas, MHD simulations have been also carried out in vacuum toroidal field and RFP-like (Reversed Field Pinch) configurations. It is found that plasmoids drift in the opposite direction of the magnetic curvature vector in the tokamak, vacuum toroidal field and RFP-like configurations. On the other hand, it is found that the drift motions depend on the initial locations of the plasmoids in LHD. The plasmid motion is mainly determined by $1/R$ force due to toroidal field and the force due to gradient of B_R^{pl} along the field, where B_R^{pl} is the major radius component of the perturbed magnetic field induced by the plasmoid. The former force implies the drift in the opposite direction of the curvature vector which is induced in the tokamak and vacuum toroidal field. Since the latter force is dominant in the cases that the plasmoids are located inside the torus in LHD, the plasmoid motions in LHD are essentially different from one in tokamak. It is also clarified that the connection length determines which force is dominant on the plasmoid motion.

author's e-mail: ishizaki@nifs.ac.jp

2. Basic Equations

Since the plasmoid has such a large perturbation that the linear theory can not be applied, a nonlinear simulation is required to clarify the behavior of the plasmoid. The drift motion is considered to be a MHD behavior because the drift speed obtained from experimental data [1] is about several % of v_A, where v_A is an Alfvén velocity. Thus, the three dimensional MHD code has been developed by extending the pellet ablation code (CAP) [3]. The equations used in code are:

$$\frac{d\rho}{dt} = -\rho\nabla\cdot\mathbf{u}, \tag{1a}$$

$$\rho\frac{d\mathbf{u}}{dt} = -\nabla p + \mathbf{J}\times\mathbf{B} + \nu\rho\left[\frac{4}{3}\nabla\left(\nabla\cdot\mathbf{u}\right) - \nabla\times\omega\right], \tag{1b}$$

$$\frac{dp}{dt} = -\gamma p\nabla\cdot\mathbf{u} + (\gamma-1)\Bigg[H + \eta J^2$$

$$+\nu\rho\left(\frac{4}{3}(\nabla\cdot\mathbf{u})^2+\omega^2\right)\Bigg], \quad (1c)$$

$$\frac{\partial\mathbf{B}}{\partial t} = \nabla\times(\mathbf{u}\times\mathbf{B}-\eta\mathbf{J}), \quad (1d)$$

$$\mathbf{J} = \nabla\times\mathbf{B}, \quad (1e)$$

$$\omega = \nabla\times\mathbf{u}. \quad (1f)$$

ρ, $\mathbf{B}$, $\mathbf{u}$ and p are normalized by ρ_0, B_0, v_A and B_0^2/μ_0 at the magnetic axis, respectively, where μ_0 is the magnetic permeability. $\gamma = 5/3$, $\nu = 10^{-6}v_A L_0$ and $\eta = 10^{-6}\mu_0 v_A L_0$ are used as the ratio of the specific heats, viscosity and electric resistivity, respectively, where L_0 is a characteristic length; 1 m. Heat source H is given by:

$$H = \frac{dq_+}{dl}+\frac{dq_-}{dl}, \quad (2)$$

where $q_\pm$ is the heat flux model dependent on electron density and temperature in the bulk plasma and the plasmoid density. l is the distance along the field line. The subscript + (−) refers to the electrons going to the right (left). Then, the heat source can be evaluated on each field line. Assuming Maxwellian electrons incident to the plasmoid, a kinetic treatment using a collisional stopping power formula leads to the heat flux model, $q_\pm$ [3] which is used in construction of the ablation model [2].

In order to investigate the plasmoid motion in LHD plasmas, an equilibrium obtained by the HINT code [7] is used as the bulk plasma. Although the HINT code uses the rotational helical coordinate system, the CAP code uses the cylindrical coordinate system (R, ϕ, Z) because of preventing numerical instability induced by a locally and extremely large perturbation of the plasmoid, where R is the major radius and ϕ is the toroidal angle. In addition, the Cubic Interpolated Psudoparticle (CIP) method is used in the code as a numerical scheme [8].

3. Drift motions of plasmoids in tokamak, vacuum toroidal field, RFP-like and LHD configurations

The plasmoid motions are different between in tokamak and LHD experiments. In order to clarify the difference and obtain the universal understanding on the plasmoid motions in torus plasmas, six simulations have been carried out as shown in Tab. 1. The magnetic configurations of cases 1, 2 and 3 are tokamak, vacuum toroidal field and RFP-like ones, respectively. Cases 4, 5 and 6 have been carried out in order to clarify the dependence on the initial locations of the plasmoids in LHD. Initial locations of the plasmoids in case 4 and 5 are respectively inside and outside the torus on the horizontal elongated poloidal cross section. The one in case 6 is inside the torus on the vertical elongated poloidal cross section.

Table 1 Simulation conditions

Case	Configuration	Plasmoid location	Poloidal cross section	Curvature vector at plasmoid
1	Tokamak	inside	—	negative
2	Vacuum	—	—	negative
3	RFP-like	inside	—	positive
4	LHD	inside	horizontal	positive
5	LHD	outside	horizontal	negative
6	LHD	inside	vertical	negative

Figure 1(a) shows a poloidal cross section of a tokamak in case 1, in which the contours and colors show the magnetic and plasma pressures, respectively. A circle is an initial plasmoid whose peak values of density and temperature of the plasmoid are 1000 times as large as density and 1/1000 times as large as temperature of the bulk plasma, respectively. The plasmoid, whose half width is 0.03, encounters the electrons with fixed temperature 2 keV and density 10^{20} m^{-3}. It is located inside the torus, namely at the high field side. A magnetic curvature vector where the plasmoid is located is negative in the major radius direction. Figure 1(b) shows the plasma beta and safety factor of the tokamak. Figures 2(a) and (b) show the simulation results in the view from the top

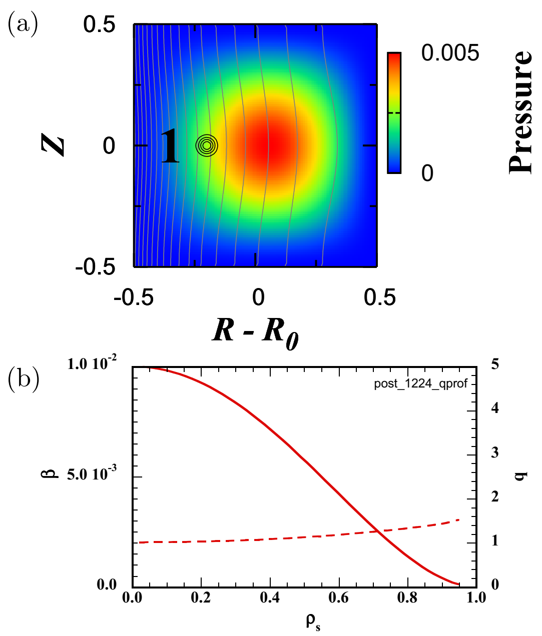

Fig. 1 (a) Poloidal cross section in case 1 where $R_0 = 1$. Contours and colors show the magnetic and plasma pressures, respectively. A circle is an initial plasmoid. (b) Plasma beta β (solid line) and safety factor q (dashed line) as a function of normalized minor radius ρ_s.

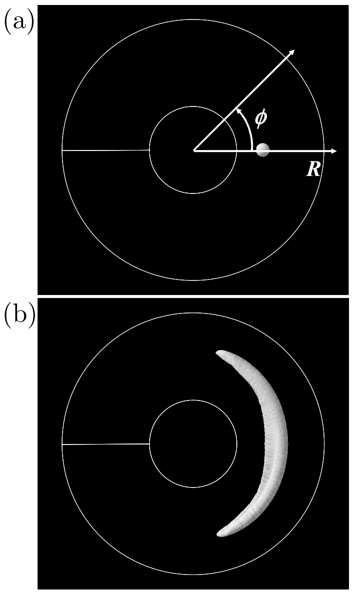

Fig. 2 View from the top of the torus in case 1. Whites show plasmoid at (a) $t = 0$ and (b) 5.

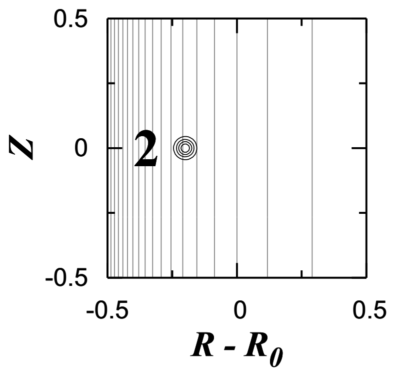

Fig. 3 Poloidal cross section in case 2 where $R_0 = 1$. Contours show the magnetic pressure. A circle is an initial plasmoid.

of the torus at $t = 0$ and 5, respectively, which is normalized by the Alfvén transit time. It is found that the plasmoid expressed by a white sphere is elongated along the magnetic field with about 25% of the Alfvén velocity and simultaneously drifts in the direction of the major radius with about 4% of the Alfvén velocity.

Figure 3 shows a poloidal cross section of a vacuum toroidal field in case 2 in which the contours show the magnetic pressure. A magnetic curvature vector at the plasmoid is negative in the major radius direction. Figures 4(a) and (b) show simulation results at $t = 0$ and 5, respectively. The plasmoid drifts in the direction of the major radius similarly to the tokamak.

Figure 5(a) shows the poloidal cross section of the RFP-like configuration in case 3. An initial plasmoid is located inside the torus. Figure 5(b) shows the plasma beta and safety factor. This configuration is not a typical RFP because it dose not have the rever-

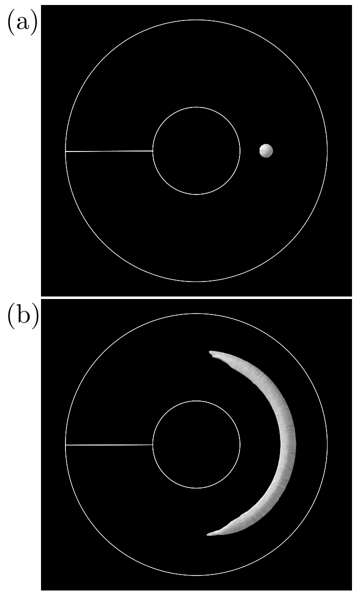

Fig. 4 View from the top of the torus in case 2. Whites show plasmoid at (a) $t = 0$ and (b) 5.

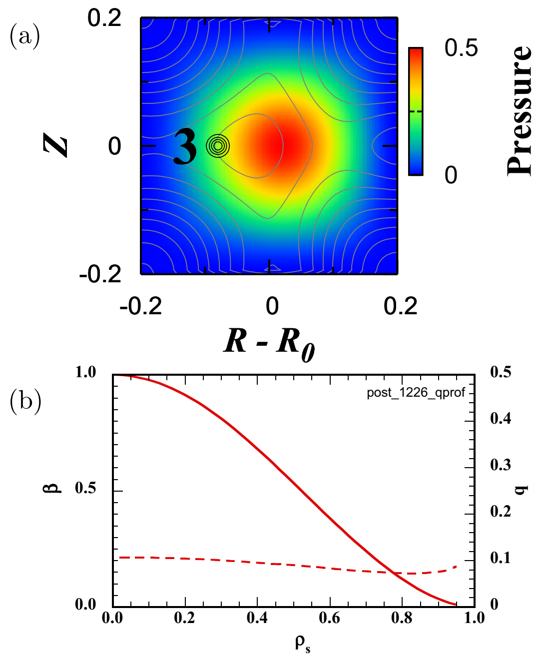

Fig. 5 (a) Poloidal cross section in case 3 where $R_0 = 1$. Contours and colors show the magnetic and plasma pressures, respectively. A circle is an initial plasmoid. (b) Plasma beta β (solid line) and safety factor q (dashed line) as a function of normalized minor radius ρ_s.

sal of the toroidal field toward the wall. On the other hand, it has the features of a typical RFP which are the toroidal field $\sim$ the poloidal field, the plasma beta, $\beta \sim 1$ and the safety factor, $q \sim a/R \sim 0.1$, where a and R are minor and major radii, respectively. Then, this configuration is called as the RFP-like one here. Figures 6(a) and (b) show the simulation results at

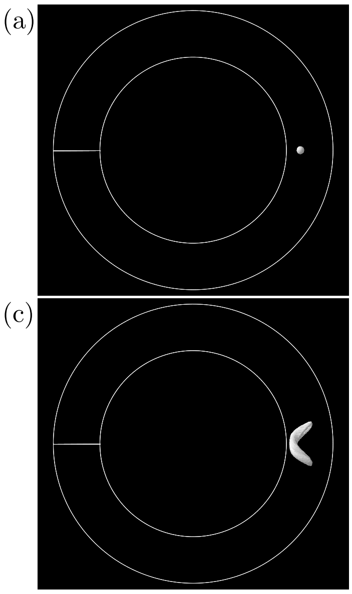

Fig. 6 View from the top of the torus in case 3. Whites show plasmoid at (a) $t = 0$ and (b) 2.

$t = 0$ and 2, respectively. The plasmoid is elongated along the magnetic field and simultaneously drift in the negative direction of the major radius. Since the RFP-like configuration has larger poloidal field and larger aspect ratio than the tokamak, the magnetic curvature is dominated by the poloidal field. Then, the curvature vector at the plasmoid is positive in the major radius direction. It is found that the plasmoids drift in the opposite direction to the magnetic curvature similarly to cases 1 and 2. The motions in cases 1 and 2 are induced by $1/R$ force and the motion in case 3 is induced by $1/a$ force due to the magnetic field [9]. The detail is discussed in the following section.

The configuration of LHD in cases 4, 5 and 6 are shown in Fig. 7. Figures 7(a) and (b) show the horizontal elongated poloidal cross section and vertical elongated poloidal cross section, respectively. Initial plasmoids in cases 4 and 5 are shown in Fig. 7(a) and one in case 6 is shown in Fig. 7(b). The plasmoids in cases 4 and 6 are located inside the torus, namely at the left hand side of the magnetic axis, and one in case 5 is located outside the torus, namely at the right hand side of the magnetic axis. The helical plasma has a saddle point of the magnetic pressure on the poloidal cross section. Since the plasmoid in case 4 is located at the lower field side than the saddle point, the curvature vector is positive in the major radius direction. On the other hand, since the plasmoid in case 5 is located at the lower field side than the saddle point, the curvature vector is negative. Since the plasmoid in case 6 is located at the higher field side than the saddle point, the curvature vector is negative. Figure 7(c) shows the plasma beta and rotational transform in LHD. The simulation results in cases 4, 5 and

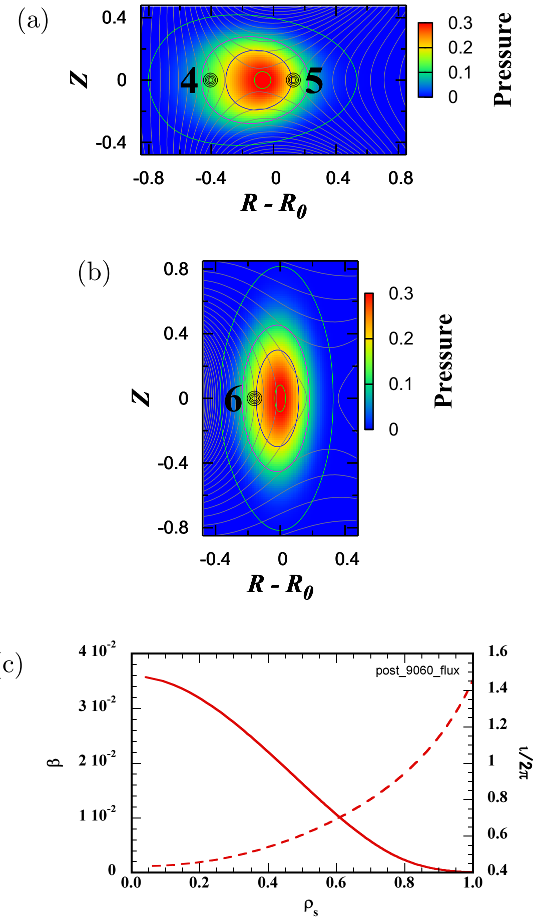

Fig. 7 Poloidal cross sections in (a) cases 4 and 5, and (b) case 6 where $R_0 = 3.82$. Contours and colors show the magnetic and plasma pressures, respectively. Circles are initial plasmoids. (c) Plasma beta β (solid line) and rotational transform $\iota/2\pi$ (dashed line) as a function of normalized minor radius ρ_s.

6 are shown in Figs. 8, 9 and 10, respectively. In case 4, the plasmoid slightly drifts back and forth in the direction of the major radius. In case 5, it drifts in the direction of the major radius. In case 6, it slightly drifts but dose not reach the magnetic axis. It is found that the results in LHD are not corresponding to ones in cases 1, 2 and 3 in which the plasmoids drift in the opposite direction to the curvature vector. The reason is discussed in the following section.

4. Discussion

The force acting on the plasmoid is given by MHD equations.

$$\begin{aligned} \boldsymbol{F} &= -\nabla\left(p^{pl} + \boldsymbol{B}^{eq}\cdot\boldsymbol{B}^{pl} + (B^{pl})^2/2\right) \\ &\quad + \boldsymbol{B}^{eq}\cdot\nabla\boldsymbol{B}^{pl} + \boldsymbol{B}^{pl}\cdot\nabla\boldsymbol{B}^{eq} \\ &\quad + \boldsymbol{B}^{pl}\cdot\nabla\boldsymbol{B}^{pl}, \end{aligned} \tag{3}$$

where $\boldsymbol{B}^{eq}$ are the equilibrium magnetic field. p^{pl} and $\boldsymbol{B}^{pl}$ are the perturbations of pressure and magnetic

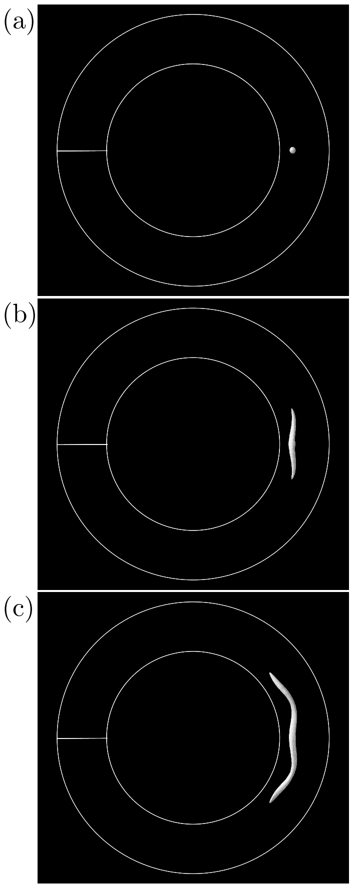

Fig. 8 View from the top of the torus in case 4. Whites show plasmoid at (a) $t = 0$, (b) 5 and (c) 10.

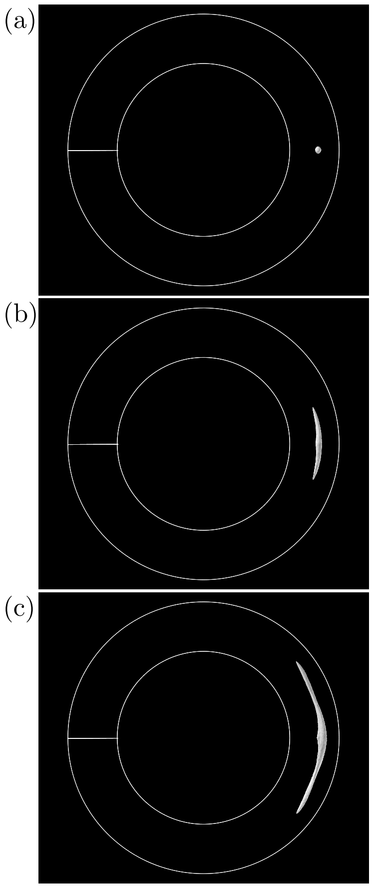

Fig. 9 View from the top of the torus in case 5. Whites show plasmoid at (a) $t = 0$, (b) 5 and (c) 10.

field, respectively, induced by the plasmoid, which are extremely large values. The first term in Eq. (3) represents the force induced by the pressure and magnetic pressure which almost cancel out each other due to the diamagnetic effect. The other terms represent the forces dominated by the magnetic curvature. Figures 11(a), (b), (c), (d), (e) and (f) show the temporal evolutions of the plasmoid accelerations induced by those forces in cases 1, 2, 3, 4, 5 and 6, respectively. The red, green, blue and pink lines show the accelerations due to the first, second, third and forth terms in Eq. (3), respectively. The sky blue lines show the total accelerations. It is found that the second terms are the leading one in all cases.

In the next step, the major radius component of the second term in Eq. (3) is decomposed as follows.

$$\begin{aligned} F_R &= \boldsymbol{e_R} \cdot \left(\boldsymbol{B^{eq}} \cdot \nabla \boldsymbol{B^{pl}} \right) \\ &= \boldsymbol{B^{eq}} \cdot \nabla B_R^{pl} - \frac{B_\phi^{eq} B_\phi^{pl}}{R}, \end{aligned} \tag{4}$$

where the cylindrical coordinate (R, ϕ, Z) is used. The first term in Eq. (4) represents the gradient of B_R^{pl} along the equilibrium magnetic field and the second term represents $1/R$ force due to the toroidal field [9]. Figures 12(a), (b), (c), (d), (e) and (f) show the temporal evolutions of the plasmoid accelerations induced by those forces in cases 1, 2, 3, 4, 5 and 6, respectively. The red and green lines show the first and second terms in Eq. 4, respectively. The blue lines show the total accelerations due to F_R. In cases 1 and 2, the second terms are dominant. On the other hand, the first terms are dominant in cases 3, 4 and 6. In case 5, it is not clear which terms are dominant. The first term in Eq. (4) can be approximately expressed by $B^{eq} B_R^{pl} / L_c$. L_c is the connection length which depends on the configuration. In the tokamak (case 1), the connection length becomes $L_c \sim \pi q R$. The second term becomes relatively larger than the first term in Eq. (4) when $q > 1$. Since the second term is always positive due to the diamagnetic effect, the plasmoid has the positive acceleration. Since the magnetic pressure is constant along the magnetic field in the vacuum toroidal field (case 2), L_c becomes infinity. Then, F_R is determined by the second term. In the RFP-like configuration (case 3), the connection length becomes short because $L_c \sim \pi q R \sim \pi a$ due to $q \sim a/R \ll 1$. Then, the first term becomes the leading one in case 3. Since the first term includes $1/a$ effect by minor radius which becomes essential in the large aspect ratio, the plasmoid motion becomes sim-

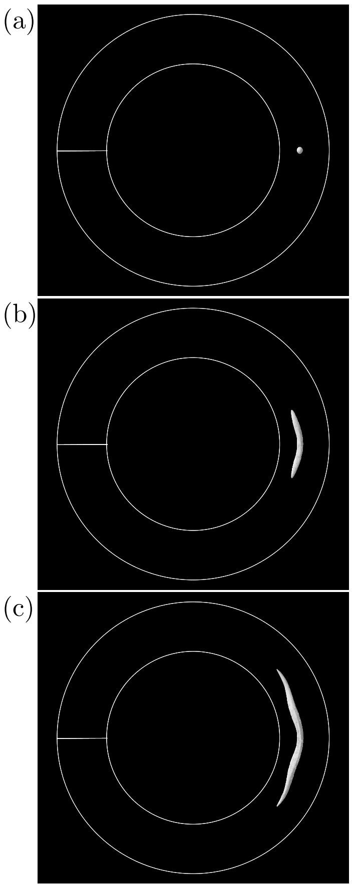

Fig. 10 View from the top of the torus in case 6. Whites show plasmoid at (a) $t = 0$, (b) 5 and (c) 10.

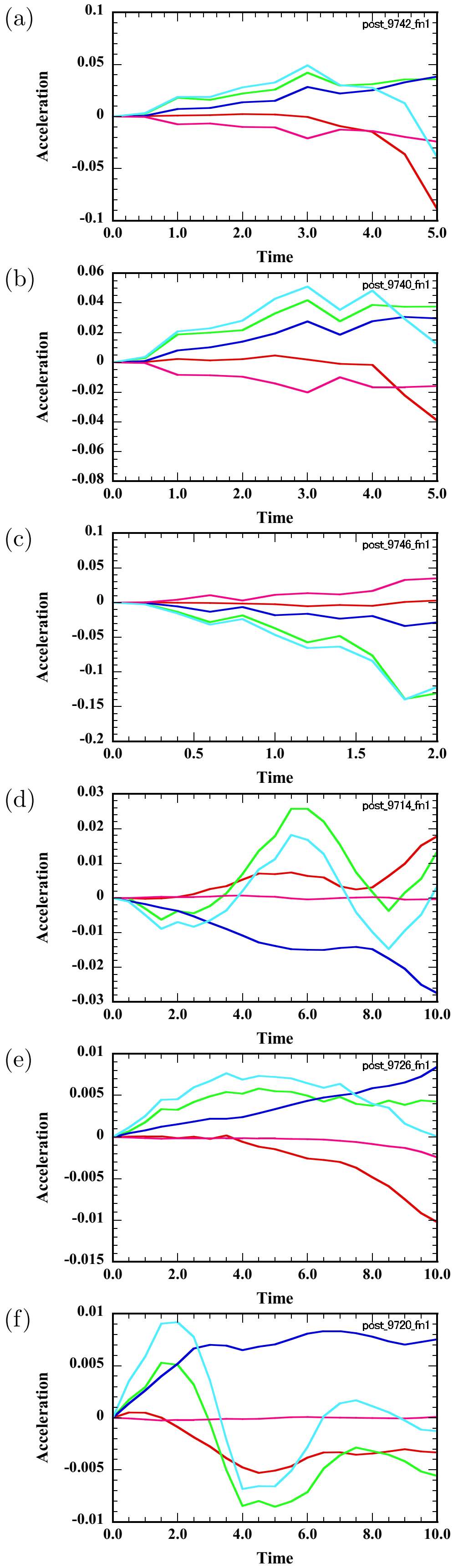

Fig. 11 The accelerations acting on the plasmoids as a function of time in cases (a)1, (b)2, (c)3, (d)4, (e)5 and (f)6. Red, green, blue and pink lines show the accelerations due to the first, second, third and forth terms in Eq. (3), respectively. The sky blue lines show the total accelerations.

ilar to the tokamak. The above evaluations of Eq. (4) are corresponding to the results in Figs. 12(a), (b) and (c). In LHD, the connection length depends on the location of the plasmoid. Figure 13 shows the spatial profile of the equilibrium magnetic pressure along the field line through the plasmoid. Red, green and blue lines are corresponding to cases 4, 5 and 6, respectively, where the plasmoids are located at $\ell = 0$. The connection length in case 5 becomes longer than ones in case 4 and 6 because the deviation of the magnetic pressure around the plasmoid is small in case 5. When this difference due to the locations is defined by $\alpha(\leq 1)$, the connection length in LHD is expressed by $L_c = \pi R/\alpha M$, where M is the toroidal pitch number, $\alpha = 1$ in cases 4 and 6 and $\alpha < 1$ in case 5. By using $M = 10$, $\alpha = 1$ and $R = 3.82$ which is the major radius at the center of the poloidal cross section, the connection length becomes ~ 1.2 which agrees with ones shown by the red and blue lines in Fig. 13. Since the first term in Eq. 4 is given by $\alpha M B^{eq} B_R^{pl}/\pi R$ in LHD, it becomes the leading one because of $\alpha = 1$ in case 4 and 6. On the other hand, both terms become dominant because of $\alpha < 1$ in case 5. Those evaluations are corresponding to the results in Figs. 12(d), (e) and (f).

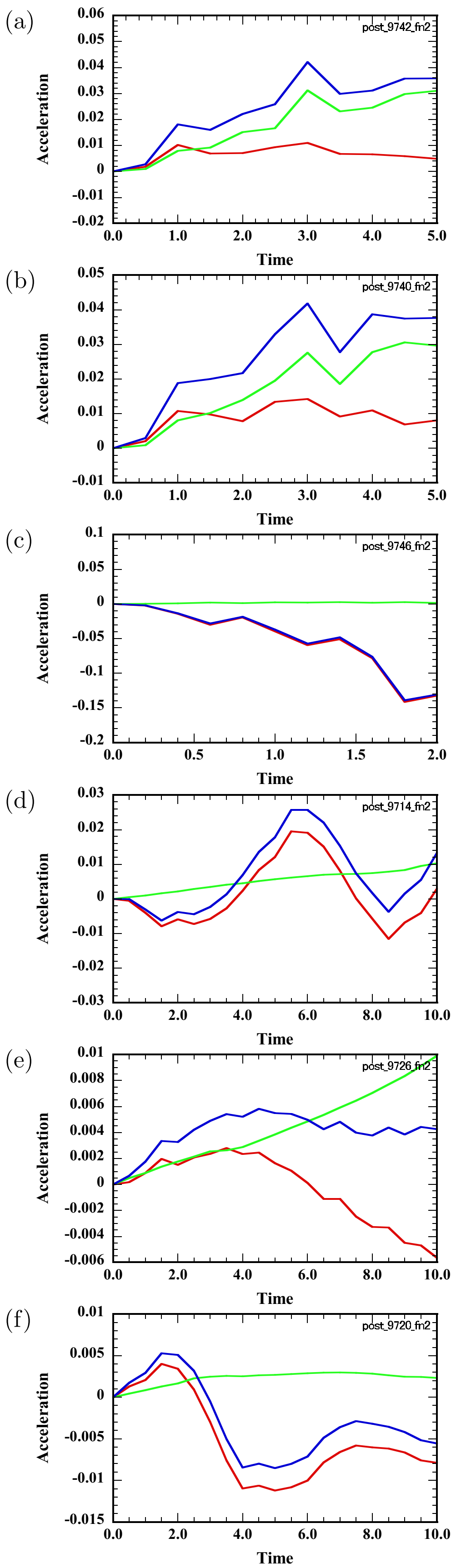

Fig. 12The accelerations due to $\boldsymbol{B_0} \cdot \nabla \boldsymbol{B_1}$ as a function of time in cases (a)1, (b)2, (c)3, (d)4, (e)5 and (f)6. Red, green and blue lines show the accelerations due to the first, second and total forces in Eq. (4), respectively.

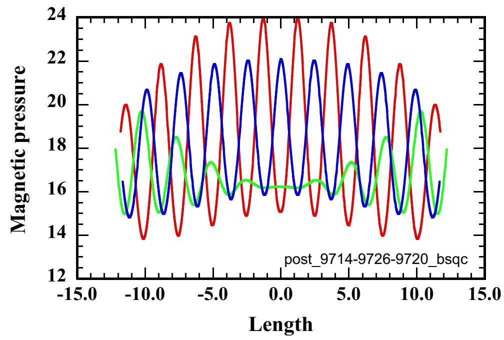

Fig. 13The equilibrium magnetic pressure, $(B^{eq})^2$ as a function of the length along the magnetic field line, ℓ. Red, green and blue lines are ones in cases 4, 5 and 6.

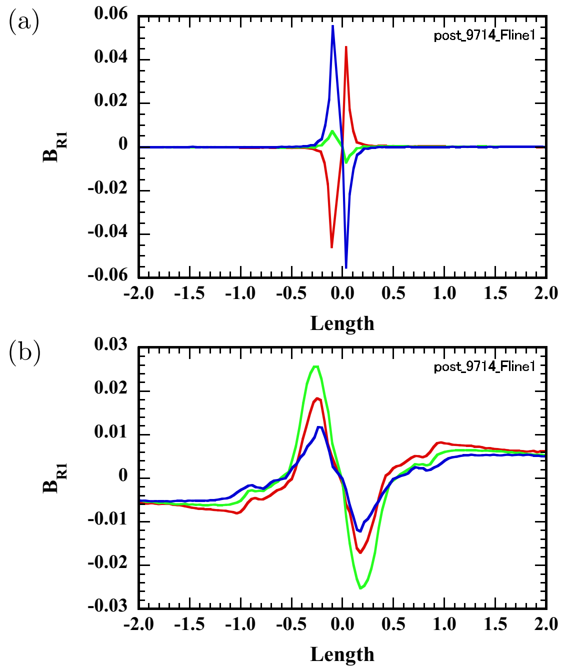

Fig. 14B_R^{pl} as a function of the length along the magnetic field line, ℓ in case 4 at (a) $t = 0.5$ and (c) $t = 2.5$. Red, green and blue lines are different field lines through the plasmoid.

There is another essence that the first terms in Eq. (4) clearly have oscillations as shown in Figs. 12(d) and (f). The plasmoid motions in Figs. 8 and 10 are induced by such oscillations. The oscillations can be explained as follows. Figure 14 shows the spatial profiles of B_R^{pl} along the magnetic field in case 4. The magnetic field lines denoted by red, green and blue are different ones through the plasmoid. The red, green and blue ones pass through $(R_{pl} - \Delta, 0, 0)$, $(R_{pl}, 0, 0)$ and $(R_{pl} + \Delta, 0, 0)$, respectively, where the center of the plasmoid is located at $(R_{pl}, 0, 0)$ in the cylindrical coordinate and Δ is a tiny value. Figures 15(a) and (b) show the physical images to understand Figs. 14(a) and (b), respectively. When we focus on the pertur-

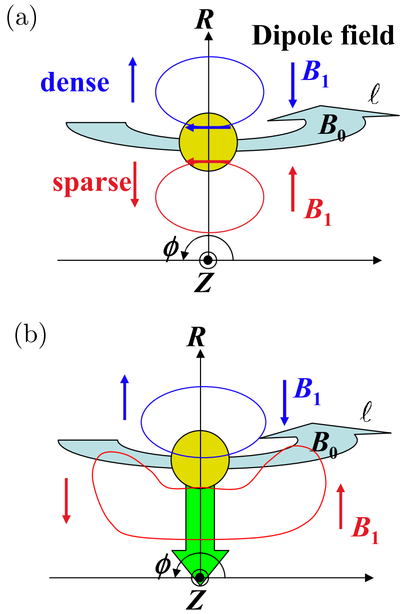

Fig. 15Physical images around the plasmoid in case 4 at (a) $t = 0.5$ and (b) $t = 2.5$.

bation of the magnetic field, the dipole fields are induced around the plasmoid by the diamagnetic effect as shown in Fig. 15(a). Since the curvature vector of the equilibrium magnetic field is positive in the major radius direction in case 4, the field lines become dense and sparse in the above region (blue line) and below region (red line), respectively, of the field line through the center of the plasmoid as shown in Fig. 15(a). Then, the magnitude of the above field line is stronger than the below one. Those physical images are corresponding to Fig. 14(a) in which the red and blue lines have opposite phases, and the absolute value of the blue line is larger than one of the red line. Subsequently, the deformation of the dipole fields is induced by the difference between the strengths of the above and below field lines as shown in Fig. 15(b). Therefore, all lines in Fig. 14(b) become same phase as the blue line in Fig. 14(a). Since $\partial B_R^{pl}/\partial\ell$ become negative on all lines, the force acting on the plasmoid becomes negative in the major radius direction according to the first term in Eq. (4). On the other hand, the magnetic field has the restoring force due to the tension. Then, the first term has oscillation in Fig. 12(d). Since the negative acceleration $(0 < t < 4)$ is slightly smaller than the positive one $(4 < t < 7.5)$ in the total acceleration as shown in Fig. 11(d), the plasmoid drifts back and forth as shown in Fig. 8. In case 6, the first term has oscillation due to the same physics. Although it continues to be negative at $t > 2$ as shown in Fig. 12(f), the total acceleration oscillates around zero as shown in Fig. 11(f) due to the increment of the acceleration by the other force. As a result, the plasmoid slightly drifts because the positive acceleration $(0 < t < 3.5)$ is slightly larger than the negative acceleration $(3.5 < t < 6.5)$ as shown in Fig. 11(f). Although the plasmoid motion is quantitatively determined by the summation of all forces, the essence of the motion is determined by the first term in Eq. (4) in cases 4 and 6. In case 5, since the first term and second term become comparable because the connection length is long as shown in Fig. 13, the plasmoid has a positive acceleration as shown in Fig. 11(e).

5. Summary

It is verified by simulations using the CAP code that the motions of the plasmoids with a high pressure induced by heat flux are different among tokamak, vacuum toroidal field, RFP-like and LHD configurations. The plasmoids drift in the opposite direction of the magnetic curvature vector in the tokamak, vacuum toroidal field, RFP-like configurations. On the other hand, in LHD, the plasmoid slightly drifts back and forth in the major radius direction when it is initially located inside the torus on the horizontal elongated poloidal cross section. It slightly drifts in the major radius direction but does not reach the magnetic axis when it is initially located inside the torus on the vertical elongated poloidal cross section. It drifts in the major radius direction when it is initially located outside the torus on the horizontal elongated poloidal cross section. The plasmid motion is mainly determined by $1/R$ force due to toroidal field and the force due to gradient of B_R^{pl} along the field. The former forces imply the drifts in the opposite direction of the curvature vector which are induced in the vacuum toroidal field and tokamak. Since the latter forces are dominant in the cases that the plasmoids are located inside the torus in LHD, the plasmoid motions in LHD are essentially different from ones in tokamak. It is clarified that the connection length determines which force is dominant on the plasmoid motion. That physics might be one inducing the difference between experiments in tokamak and LHD. In RFP-like configuration, although the former force is dominant, the plasmoid drifts in the opposite direction of the curvature vector similarly to tokamak due to the minor radius effect including in the former force.

[1] Y. W. Muller et al. Nucl. Fusion, **42**, 301 (2002).
[2] P. B. Parks and M. N. Rosenbluth. Phys. Plasmas, **5**, 1380 (1998).
[3] R. Ishizaki et al. Phys. Plasmas, **11**, 4064 (2004).
[4] P. B. Parks et al. Phys. Rev. Lett., **94**, 125002 (2005).
[5] R. Sakamoto et al. *in proceedings of 29th EPS conference on Plasma Phys. and Control. Fusion.*
[6] R. Ishizaki et al. IAEA-CN-149/TH/P3-6 (2006).
[7] K. Harafuji et al. J. Comp. Phys., **81**, 169 (1989).
[8] H. Takewaki et al. J. Comput. Phys., **61**, 261 (1985).
[9] J. P. Freidberg, *Ideal Magnetohydrodynamics* (Plenum Press, New York, 1987).